Morphology, Crystalline Features and Tensile Properties of Syndiotactic Polypropylene Blends

Le Thuy Truong[1,2], Åge G. Larsen[1*], and Jaan Roots[2]

[1]SINTEF Materials and Chemistry, P.O. Box 124 Blindern, NO-0314 Oslo, Norway.

[2]University of Oslo, Department of Chemistry, P.O. Box 1033 Blindern, NO-0315 Oslo, Norway.

* Correspondence to: Åge G. Larsen (email: age.larsen@sintef.no)

Abstract

Syndiotactic polypropylene (sPP) was modified with ethylene-octene copolymer (EOC), ethylene-propylene rubber (EPR) with test samples prepared in a twin-screw extruder and then injection moulded. Phase morphology, rheology, thermal and tensile properties of the modified sPP was investigated. Atomic Force Microscopy studies show how phase morphology of sPP blends with elastomers depends on blend compositions and results compares with the storage modulus at low frequency. EOC and EPR are dispersed phase in sPP matrix with spherical shapes when dispersed content is 20 wt% and lower. The phase co-continuity starts at around 40 wt% of EOC for sPP/EOC blends and around 60 wt% of EPR for sPP/EPR and the dispersed phase forms more complex elongated shapes. Rheological and thermal properties are affected by the sPP-elastomer interphase. EOC promote crystallization of sPP, increasing crystallization temperature and rate. In contrast, EPR gives an opposite effect on crystallization behavior and the results indicate that sPP and EPR are not completely separated. Tensile properties were studied from -20 °C to 100 °C. We find that tensile properties at low temperature may be improved without loosing high temperature properties. In the particular case of 20 wt% of EOC, both the strain at yield and at break of the sPP/EOC blend are improved both at -20 °C and at 100 °C.

Keywords: Polyolefins, elastomers, morphology, crystallinity, mechanical properties

1. Introduction

As new metallocene catalysts have been developed, syndiotactic polypropylene (sPP) with high tacticity has been commercially produced. This sPP exhibits remarkable physical and mechanical properties such as toughness and good elastic behaviour [1]. Cable insulation is one possible application of sPP. In comparison with isotactic polypropylene (iPP), sPP shows a more fine grained morphology [2-6] which contributes to better electrical characteristics. sPP has also better electrical and mechanical properties at high temperature than cross-linked polyethylene (XLPE) [4]. Compared to the conventional insulation material XLPE, sPP, which is not cross-linked, will also be suitable for recycling.

One challenge for sPP relates to slow crystallization rate which limits commercial application of this polymer [7-10]. In addition, sPP has a relatively high brittleness temperature which would limit low temperature applications.

Aiming to improve sPP properties there is a lot to learn from previous work on iPP. Much focus in the previous work on iPP has been on modifying blend composition and morphology to improve impact properties and low temperature properties.

Extensive research has been published on the blends of isotactic polypropylene with ethylene-propylene rubber (EPR) [11,12] and ethylene-propylene-diene terpolymer (EPDM) [13-15]. More recently, ethylene-octene copolymer (EOC) has attracted attention by many researchers [16-18]. In [17] properties were studied at room temperature and mechanisms for improved toughness were identified. EOC/iPP blends exhibited good elastic behaviour and elongation and in the case of 40% of PP, the morphology resembled a co-continuous one [18]. Ternary

systems have also been studied. In [19] it was demonstrated how mechanical and optical properties were improved by blending a crystalline polypropylene with EPR or EPC and styrene-butadiene elastomer (SEBS) by selective choice of the SEBS type.

Knowledge of phase continuity is very important for polymer blends because it is related to mechanical properties. Heterogeneous phase morphologies are commonly achieved since most polymer blends are immiscible or partly miscible. Blend properties are determined by the characteristics of each component plus interphase and by phase morphology developing during melt mixing process. A wide range of characterization methods has been applied to the study of polymer blends such as transmission electron microscopy (TEM), scanning electron microscopy (SEM) and solvent extraction. Atomic force microscopy (AFM) is a convenient method compared to TEM and SEM in sense of easier sample preparation. Due to the strong modulus contrast between elastomer and PP, tapping mode AFM is an excellent tool in evaluating the morphologies of polymer/elastomer blends [12]. Dynamic rheology, and in particular the storage modulus at low frequencies has shown a reliable tool to determine the co-continuity on binary blends [20].

Modification of syndiotactic polypropylene has also attracted interest of researchers during the last decade in order to improve physical and mechanical properties and thus broaden commercial applications of sPP [2,3,21-23]. The continuous developments of sPP-based materials by inorganic nanoparticles incorporation or blending with other materials are the most popular modification routes reported.

Copolymers of sPP and alpha-olefins showed decreased stiffness and microhardness as well as the brittle–ductile transition temperature (BDTT) [24].

Yoshino et. al. blended elastomers into sPP [4]. Their blends with VLDPE and especially polyolefin elastomer (POE) gave significantly improved brittleness temperature compared to that of pure sPP.

The morphology and crystallization kinetics of sPP/ alumina nanocomposites were previously studied in our laboratory [2,3,23]. In [3] we showed that alumina nanoparticles improves crystallization rate of sPP which adds to the present study.

In this study, blends of sPP with two elastomers; EPR and EOC, were investigated. Phase morphology, phase inversion points and crystallization of the two blends were studied by AFM and dynamic rheology. Tensile and thermal properties of the modified syndiotactic polypropylenes at low and high temperature were also measured.

We find that blending may improve low temperature tensile properties while maintaining properties at high temperature. The storage modulus G' increases, when a softer elastomer is added. Comparing the phase morphology with variations in G', interphase properties appear to explain the results. EOC is found to increase both nucleation temperature and crystallization rate of sPP. Blends with EPR have both lower nucleation temperature and crystallization rate.

2. Experimental

2.1. Materials

Commercial syndiotactic polypropylene (Total 1471) used in this work was supplied by Total Fina, France. Ethylene propylene rubber (Versify 3300) and ethylene-octene copolymer (Engage 8450) were obtained from Dow Chemicals, US. Engage 8450 is produced using metallocene catalyst. This was chosen since metallocene catalysed polyethylene has proven effective in impact toughening of iPP [25]. Materials data are given in Table 1. Notice the different reference temperatures for melt flow rate measurements.

Table 1 Melt flow rate, density and flexural modulus of the polymers studied

Materials	**Melt flow rate ***	**Density/ (g/cm^3)**	**Flexural modulus / (MPa)**
Syndiotactic polypropylene (sPP)	4/230	0.88	340
Ethylene propylene rubber (EPR)	8/230	0.87	35
Ethylene–octene copolymer (EOC)	3/190	0.90	78

** at 2.16 kg (dg/min) /temperature (*°C)

2.2. Sample preparation

The sPP and elastomer (EOC or EPR) were manually premixed, and the mixture was melt blended in a co-rotating twin batch screw extruder (DSM Midi 2000) at 70 rpm and 200 °C for 3 min. The content of EOC or EPR was varied from 0 to 100 wt% in the blends. The extruded samples were then moulded in a lab-scale injection moulding machine. The mould temperature was 40 °C.

2.3. Characterization

Rheological analysis: Disk-like samples for rheological analysis were prepared by using injection moulding at 8 MPa. Temperature at cylinder and mould is 200 °C and 40 °C, respectively. The thickness and diameter of samples were 2 and 25 mm, respectively. A rotational rheometer (Physica MCR-300, Anton Paar) was employed for rheological experiments. All tests were carried out by using 25 mm parallel plates with a gap of 1.4 mm at 200 °C under nitrogen gas. Strain sweep showed that the viscoelastic behaviour of the blends to be linear up to strain amplitude of 10% except for sPP/EPR (20/80). Frequency sweep measurements were performed at strain amplitude of 0.1 % for sPP/EPR (20/80) and 1 % for the rest of specimens in order to investigate the rheological behaviour within the linear viscoelastic region. The angular frequency range investigated was from 0.01 rad/s to 500 rad/s.

Atomic force microscopy: Dumbbell specimens were microtomed perpendicularly to injection direction at -100 °C by using a Reichert Ultracut S ultramicrotome equipped with a glass knife to create a plane surface. All AFM measurements were analyzed on a Nanoscope IIIa controller (Veeco, USA) using manufacturer supplied software. Tapping mode was performed using silicon tips with force constants of 20-80 N/m and a resonant frequency of approximately 265-400 kHz. The tip was oscillated below the resonant frequency to maintain a good contact with the surface. We exclusively used the images where the harder sPP phase was inferred by a bright color. Images were flattened using the instrument built-in image processing software. ImageJ [26] was applied for phase study for sPP/EPR blends. Firstly, AFM images were split into three separate color channels (red, green and blue) by using split

channels. The green channel was selected to increase the contrast between phases. Finally the images were made binary where we can see only black and white areas.

A Differential Scanning Calorimeter (DSC), Perkin–Elmer Pyris 8500, was applied to record melting and crystallization behaviours for these resins. Calibration for the temperature and heat flow was carried out using both an indium standard (melting temperature 156.6 °C and ΔH = 28.5 J/g) and a zinc standard (melting temperature 419.47 °C and ΔH = 108.37 J/g). Standard aluminium pans (PerkinElmer 0219-0041) were used to minimize thermal lag between the polymer sample and the DSC furnace. Sample sizes were 2-4 mg. All measurements were carried out under nitrogen atmosphere. The crystallization experiments started with heating each sample from 20 to 200 °C at a heating rate of 40 K/min and holding at 200 °C for 5 min in order to set a similar thermal history to all samples. The sample was then crystallized at 10 K/min. Melting thermograms were recorded at a heating rate of 250 K/min in order to avoid recrystallization.

Tensile tests according to DIN EN ISO 527-1 standards were performed using a test machine, Zwick/Roell Z250, Germany. Dumbbell specimen type 1BA was produced by injection moulding. All samples had been stored in an acclimatized room (23 °C, 50 % humidity) for at least 24 hours before testing. The test was conducted by following parameters: a pre-load of 5 N; a speed for tensile modulus of 1 mm/min; a test speed of 500 mm/min; a grip distance of 50 mm, gauge length of 25 mm. Testing temperature was -20 °C, 0 °C, 23 °C, and 100 °C. For low temperature testing, -20 °C and 0 °C, liquid nitrogen was used in the chamber. Samples were stored in the testing chamber at required temperature for at least an hour before testing. For testing at 100 °C, the chamber was heated up to 100 °C for 30 minutes, and then

samples were mounted on the upper grip and left to condition for 3 min before testing. At least five specimens of each composition were tested and the average values reported.

3. Results and Discussion

In comparing EOC and EPR in order to understand the blend properties, the complex viscosity at low and high angular frequency in addition to the phase images gives necessary information. The datasheet MFR's in Table 1 cannot be directly compared as they are measured at different temperatures.

Fig. 1 (A-C) shows the complex viscosity and the storage modulus (G') as a function of angular frequency. Fig. 1 (A) shows that the results for 20 wt% EPR blend almost overlaps the sPP results, whereas the EOC blend differs significantly at low frequencies. The blends cannot be assumed to the rheological simple fluids as activation energies are different for PP and ethylene and we also have an interphase with unknown properties. Thus the Cox-Merz rule does not apply and the complex viscosity for the blends cannot be assumed equal to the shear viscosities.

All the materials exhibited “shear thinning” behaviour. In general, complex viscosity of sPP/EPR and sPP/EOC blends is decreased with increasing elastomer content. However, as the content of EOC is 20 wt% or lower the complex viscosity of sPP/EOC blends is increased at low angular frequencies compared to pure sPP.

For the pure elastomers, at ω=0.1 rad/s, EPR has highest complex viscosity but from around ω=1 rad/s and up, viscosities are equal. sPP/EPR and sPP/EOC blends possess a Newtonian

plateau as seen in Fig. 1 (A). For EOC blends, this limit is reached at a lower angular frequency. The sPP blends with 20 wt% of EOC has the highest complex viscosity and highest G' of all the polymers.

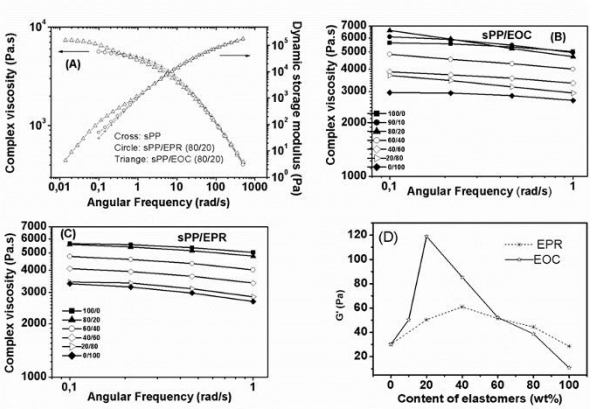

Figure 1. The complex viscosity and dynamic storage modulus vs. angular frequency for sPP and sPP blends with the blending ratio of 80/20 (A). Comparison of complex viscosity of various contents of elastomers at low angular frequency: sPP/EOC (B) and sPP/EPR (C). The storage modulus (G') at angular frequency 0.1 rad/s as a function of composition of sPP/EOC and sPP/EPR (D)

The interesting differences at low ω between EOC and EPR blends up to 20 % elastomer content do not relate to an increased "efficient" molecular weight for the 10 and 20 % EOC blends. The dynamic measurements involve small deformations and may probe interphases and not bulk properties. Thus, the results in Fig. 1 (B) may show effects of surface tension between sPP and the elastomers. This also relates to the phase distribution of the blends as discussed next.

The effect of elastomer content on storage modulus (G') at angular frequency 0.1 rad/s is presented in Fig. 1 (D). We notice that G' for EOC blends reach twice the level of that of the EPR blends. Thus, sPP-EOC interphase shows very different properties compared to the

interphase of sPP-EPR blends. Incorporation of softer elastomers leads to an increase in G' of the polymer blends. Figs. 2, 3 and 4 show AFM tapping mode micrographs of sPP blends with different elastomer content. A two-phase morphology was observed for all samples. In the AFM images, dark areas are associated with the softer EOC or EPR. For selected cases we applied image analysis (ImageJ) to see which phase is the dispersed. Fig. 5 shows binary images derived from the AFM images in Figs. 2 and 4.

The maxima of elasticity at 20 and 40 wt% for EOC and EPR respectively, correspond to the onset of the continuity of the minor phase [20]. G' increases with EOC content up to 20 wt% EOC loading and the storage modulus shows a maximum with an increase of about 300 % as compared with virgin sPP.

In [20] the presence of a second peak in the G' plot was discussed, giving the limit of the co-continuity interval. In our data this is rather weak but there might be signs of peaks around an elastomer content of 80 wt%.

The EOC elastomer is well dispersed within the sPP matrix as can be seen in Figs. 2 and 3. In general, domain sizes will depend on viscosity and interfacial tension. The increase of the storage modulus is related to the interface surface area and the properties of the sPP-elastomer interphase. Beyond 20 wt% EOC content, a decline in G' of the blends is observed. At 40 wt% EOC content, Fig. 2 (C), we see that EOC domains are merged and correspondingly interfacial surface area is decreased. From this point, the influence of the softer elastomer on blend properties increases.

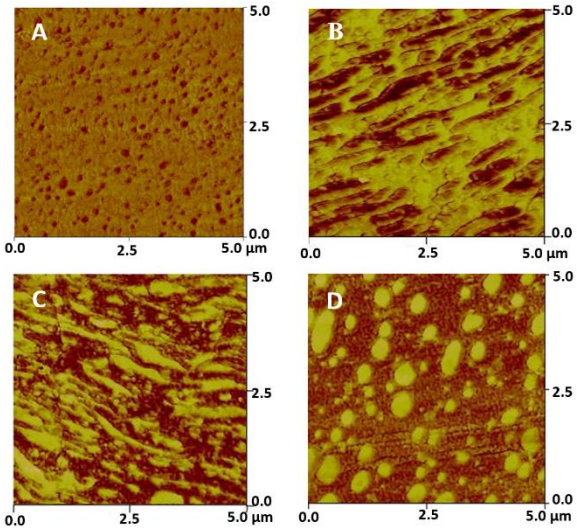

Figure 2. AFM micrographs of sPP/EOC blends at various compositions (wt/wt): 90/10 (A), 60/40 (B), 40/60 (C) and 20/80 (D)

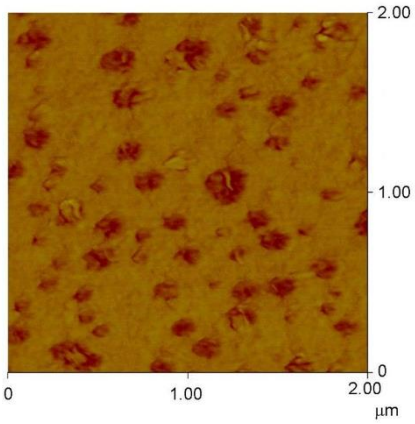

Figure 3. AFM micrograph of sPP/EOC 80/20 blend.

For sPP/EPR blends, at 40 wt% EPR, in Fig. 4 (C) and Fig. 5 (C) we see that the minor EPR phase is well dispersed. The maximum of G' obtained is less pronounced than with EOC with G’ at the maximum twice high as that of neat sPP.

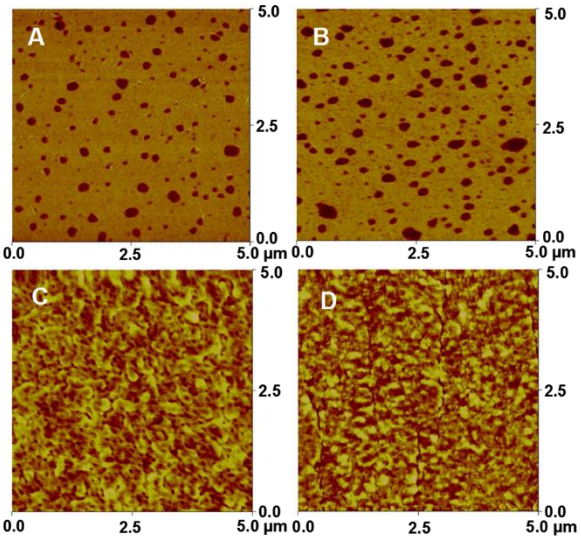

Figure 4. AFM micrographs of sPP/EPR blends at various compositions (wt/wt): 90/10 (A), 80/20 (B), 60/40 (C) and 40/60 (D).

For 10 and 20 wt% of elastomer content, the EOC domains are smaller than EPR domains. Inside the EOC phases at 20 wt% of elastomer content in Fig. 3, there are islands of harder material, whose contrast is very similar to the matrix. See also Fig. 5 (A). This core-shell structure is not clearly observed at lower EOC levels. Using tapping mode AFM, Tanem et al. reported that the hard inclusions in the segregated phase are ethylene crystals [12]. At 40 % of EOC, the majority of EOC particles are elongated, and EOC is present both as the dispersed and continuous phase. At 60 wt% of PP, the sPP and EOC phase distribution is close to co-continuous, although sPP is partly dispersed. At 80 % of EOC the situation is reversed: EOC become a matrix and sPP is fully dispersed and formed small droplets. The phase morphology also depends on the blend concentration, Figs. 2 and 3. At low concentration the minor phase forms nearly spherical drops, but at higher loading elongated structures are formed.

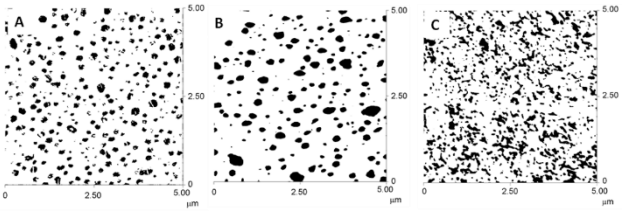

Figure 5. Image analysis for AFM micrographs of sPP/EOC (80/20) blend (A), sPP/EPR (80/20) blend (B), and sPP/EPR (60/40) blend (C).

In Fig. 4, we show AFM tapping mode micrographs of sPP blends with increasing EPR concentration with 10, 20, 40, and 60 wt% of EPR. When the EPR level is 20 wt% or lower, the matrix is sPP and the dispersed phase is EPR, Figs. 4 (B) and 5(B). At 40 % EPR, Fig. 5(C), the EPR is dispersed and there is no dominant elongation of EPR phase. At 60 wt% of EPR, the structure is close to co-continuous, Fig. 4(D).

Based on the morphology results above, we have chosen 10 and 20 wt% of elastomers for tensile properties later on. With these compositions, elastomers are dispersed in sPP matrix, and thus mechanical properties of blend should mainly be governed by the properties of the sPP matrix.

Fig. 6 presents the melting curves of neat sPP, EOC, EPR the blends sPP/EOC and sPP/EPR at heating rate 250 K/min. At such high heating rate, recrystallization of sPP is avoided, and thus the heat flow curves reflect the crystallinity of the materials resulting from the processing conditions. EOC melts over a wide range and the two melting endotherms of the sPP/EOC blends corresponds to this effect of EOC on sPP. A low temperature shoulder is seen around 104 °C.The melting temperature of sPP in sPP/EOC blends shifts toward higher temperature with the addition of EOC. With EPR as minor component only one peak can be seen and the melting temperature is lower. Neat EPR does not show any melting peak at all in this test.

From Fig. 6, the melting temperature for the neat sPP is 118.0 °C, and shifts to higher temperature, 118.6 °C and 120.4 °C, with 10 and 20 wt% of EOC content, respectively. For the sPP/EPR blends, the melting temperature for the (90/10) case is 116.2 °C and for (80/20) 114.1 °C. The changes in melting temperatures should relate to the properties of the interphases for the sPP/EOC and sPP/EPR blends. The increase in melting temperature of sPP in sPP/EOC blends indicate sPP crystals are more stable in the presence of the EOC. As melting temperature relates to lamellar thickness which increases with crystallization temperature this indicates that crystallization initiates at a higher temperature in this case

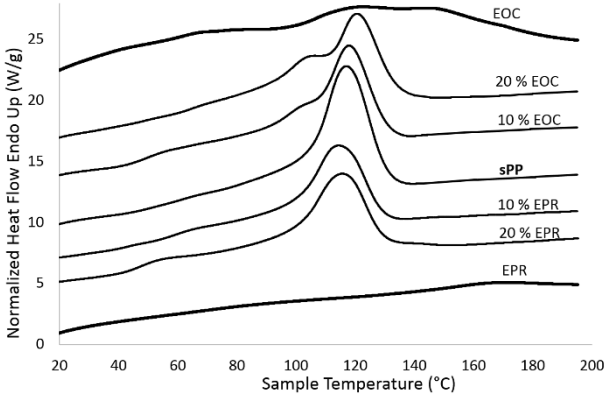

Figure 6. Melting curves of sPP, EOC and EPR and blends

Fig. 7 (A) shows the non-isothermal crystallization behaviour under cooling at 10 K/min of sPP, EOC, EPR the blends sPP/EOC and sPP/EPR. From the DSC crystallization thermograms, the relative crystallinity $X_t(T)$ as a function of temperature can be calculated by integrating the heat flow as given in Equation (1):

$$X_t(T) = \frac{\int_{T_0}^{T} (dH_c / dT) \times dT}{\int_{T_0}^{T_\infty} (dH_c / dT) \times dT} \qquad (1)$$

Here T_0, T and T_∞ correspond to the crystallization onset, experimental temperature and temperature where complete crystallization occurs, respectively; dH_c/dT represents the change of the crystallization enthalpy as a function of temperature; and ΔH_c, the overall

crystallization enthalpy under cooling. Fig. 7 (B) shows the development of the relative crystallinity X_t as a function of temperature during cooling for the material combinations in Fig. 7 (A) for sPP and the blends.

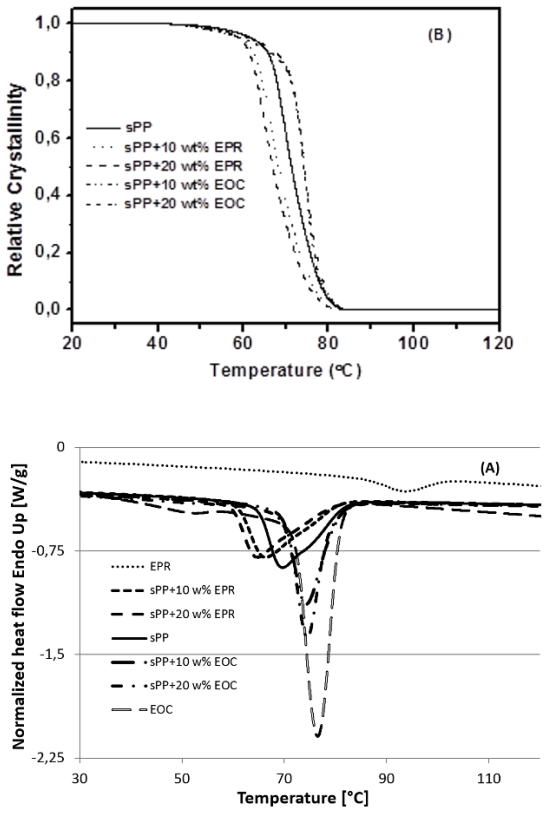

Figure 7. (A) Non-isothermal crystallization curves of sPP, EOC, EPR and blends. (B) Relative crystallinity as a function of temperature of sPP and blends.

In Fig. 7A we see the weak crystallization peak of EPR around 94 °C while EOC has a pronounced peak at 76,6 °C. From Figs. 7 A and B we see that the presence of EOC shifts the crystallization peak to a higher temperature but does not influence the nucleation temperature and that the nucleation temperature is the same for neat sPP, neat EOC and EOC blends. The faster crystallization shows that the crystallization of the sPP matrix is influenced by EOC and as EOC forms separate domains this must be by crystallization at the phase boundary.

Crystallinity is increased with increasing EOC content but the peak temperature is the same at the two different concentrations. In contrast to EOC, the presence of EPR in sPP blends decreases the nucleation temperature, the crystallization temperature and the crystallization enthalpy. This is surprising considered the higher crystallization temperature of EPR. It may reflect differences in interphase properties for blends with EOC compared to blends with EPR as was also concluded from the dynamic measurements. The higher EPR content, the lower peak temperature and enthalpy is observed.

The shifts in melting peak temperatures in Fig. 7 (A) are reflected by variations in the slope of the X_t (T) curves in Fig. 7 (B).

The observed shifted and sharper crystallization peaks for EOC blends is similar to observations on iPP/EOC blends [27]. With EOC content higher than 20 wt%, the crystallization of iPP was hindered, and thus the crystallization temperature decreased since there is competition between nucleation and retarding crystallization of iPP in iPP/EOC blends [27]. In our observation on sPP/EPR blends with the lower crystallization temperature than sPP, the effect may indicate a degree of miscibility between sPP and EPR. Nucleation temperature is close to that of EOC but growth occurs at a lower temperature. This agrees with previous observations of crystallization of blends of metallocene polyethylene and PP [28].

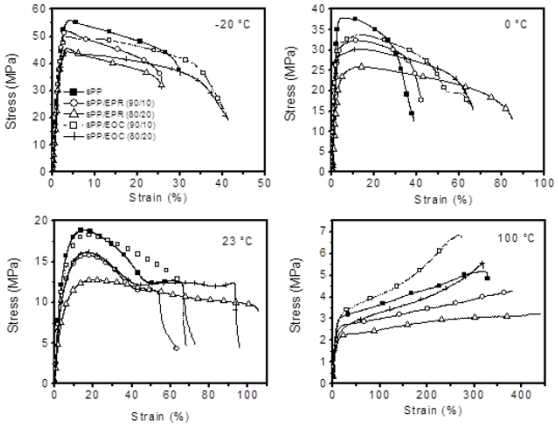

Figure 8. Stress–strain curves of neat sPP and sPP blends at different testing temperatures.

Fig. 8 illustrates tensile measurements of neat and modified sPP. Samples for tensile studies were syndiotactic polypropylene blends with 10 and 20 wt% of elastomers. It is seen that the neat sPP and the modified sPP with a rich proportion of sPP showed a well-defined yield point at low temperature and room temperature. However, at high temperature, 100 °C, the yielding phenomenon disappeared. Since it is often difficult to pinpoint the exact stress at which plastic deformation begins, the yield stress is often taken to be the stress needed to induce a specified amount of permanent strain, typically 0.2 %. A line of curve slope (modulus, E) is drawn from the strain axis at 0.2 % of strain; this is the unloading line that would result in the specified permanent strain. The stress at the point of intersection with the stress-strain curve is the offset yield stress.

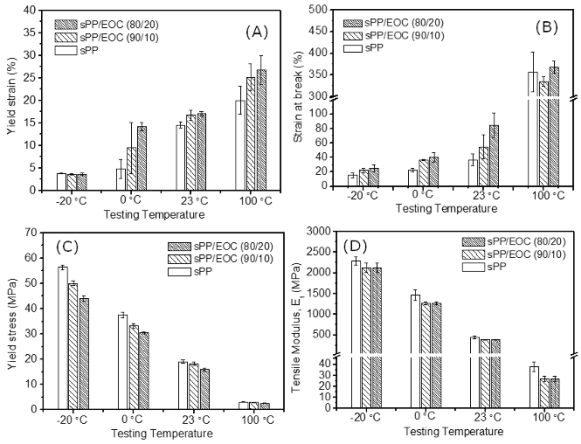

Figure 9. Effect of EOC on tensile properties of sPP at different testing temperatures.

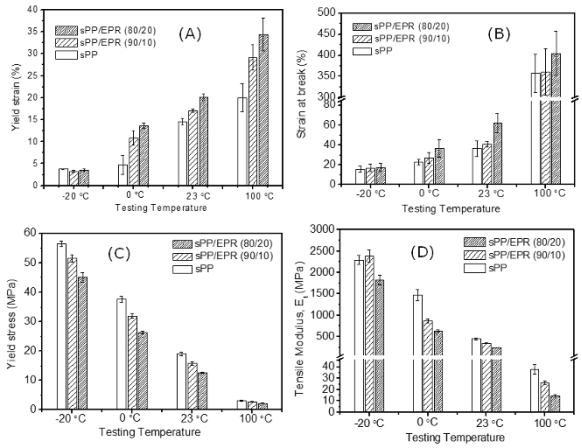

Figure 10. Effect of EPR on tensile properties of sPP at different testing temperatures.

Average results of tensile testing at various temperatures are presented in Figs. 9 (EOC) and 10 (EPR), showing comparisons of tensile modulus, stress and strain at yield and break point of sPP and modified sPP at different testing temperature. As was to be expected, tensile modulus, yield stress and stress at break decreased while strain at both yield and break increased with increasing elastomer content and temperature. Yield strains and strain at break are improved for both elastomers down to 0 °C. For EOC strain at break is also improved at -20 °C. EPR yields a higher reduction in tensile modulus than EOC as could be expected from

the data in Table 1. From the data presented, we cannot relate differences in properties to the differences in crystallization as seen in Fig. 7A.

Conclusions

Our study has revealed essential features of the blends of sPP with EOC and EPR. The materials were not fully miscible and distinct two-phase morphology was observed for all blends with elastomer content 10, 20, 40, 60 and 80 wt%.

The co-continuity interval as found from AFM micrographs correlate with the changes in storage modulus G' with increasing elastomer content. Including small amounts of elastomer gives increased G' but passing a certain level G' is reduced. The reduction in G' relates to formation of larger elastomer domains which imply lower interface area. The properties of the sPP-elastomer interphase seem to strongly influence both the dynamic rheology and the crystallization.

Onset of co-continuous phase starts around 40 wt% of EOC in sPP. At low EOC fraction, EOC was dispersed in the sPP matrix. From 60 wt% EOC content EOC forms a continuous phase and at 80 wt% of EOC sPP is the dispersed phase. For sPP/EPR blends, the phase co-continuity starts taking place at 60 wt% of EPR.

The addition of EOC significantly increases the crystallization rate and temperature compared with sPP. The nucleation temperature is not significantly changed by the presence of EOC which means that the crystal growth of sPP is affected in the presence of the EOC. In contrast

to EOC, the presence of EPR reduces nucleation temperature, crystallization rate and crystallinity of sPP. This indicates a certain degree of miscibility between sPP and EPR on a length scale not reflected by the AFM images.

sPP blends with EOC and EPR content 10 and 20 wt% were chosen for tensile studies. While G' increases by including up to 20 % EOC or EPR, E-modulus is decreased. This reflects that dynamic testing involves much smaller deformations than tensile testing and exploits the effects of morphology on a smaller length-scale. Very interesting results in this study are that tensile properties of sPP blends were improved at low temperature while maintained at high temperature. sPP blends with 10 wt% of EOC show the same yield stress and higher stress at break compared with sPP at 100 °C.

Acknowledgements

This work is part of the Petromaks project "Electrical Insulation Materials and Insulation Systems for Subsea High Voltage Power Equipment" funded by the Research Council of Norway and the industrial partners Deutsch, Nexans Norway AS, Statoil ASA, Total E&P Norge AS and Vetco Gray-Ge Oil and Gas. Support from SINTEF Materials and Chemistry is also gratefully acknowledged.

Thanks to Frode Grytten for tensile properties' discussions, Einar L. Hinrichsen and Britt Sommer for the rheology experiments and contributions.

References

[1] C. D. Rosa, F. Auriemma, Prog. Polym. Sci. **2006**, 31, 145-237.

[2] L. T. Truong , Å. Larsen, B. Holme, F. K. Hansen, J. Roots, Polymer **2011**, 52, 1116-1123.

[3] L. T. Truong, Å. Larsen, B. Holme, J. Roots, J. Appl. Polym. Sci. **2012**, 126, 1198-1206.

[4] K. Yoshino, T. Demura, M. Kawahigashi, Y. Miyashita, K. Kurahashi and Y. Matsuda, El. Eng. Japan **2004**, 146, 18-26.

[5] K. Yoshino, A. Ueda, T. Demura, Y. Miyashita, K. Kurahashi and Y. Matsuda, Proceedings of the 7th International Conference on Properties and Applications of Dielectric Materials, Nagoya **2003**, 175-178.

[6] K. Kurahashi, Y. Matsuda, Y. Miyashita, T. Demura, A. Ueda, K. Yoshino, El. Eng. Japan, **2006**, 155, 1-8.

[7] P. Supaphol, P. Thanomkiat, R.A. Phillips, Polym. Test. **2004**, 23, 881-895.

[8] M. Grasruck, G. Strobl, Macromolecules **2003**, 36, 86-91.

[9] J. Schmidtke, G. Strobl, T. Thurn-Albrecht, Macromolecules **1997**, 30, 5804-5821.

[10] H. Uehara, Y. Yamazaki, T. Kanamoto, Polymer **1996**, 37, 57-64.

[11] N. Mnif, V. Massardier, T. Kallel and B. Elleuch, Polym. Adv. Technol. **2010**, 21, 896-903.

[12] B. S. Tanem, T. Kamfjord, M. Augestad, T. B. Løvgren, M. Lundquist, Polymer **2003**, 44, 4283-4291.

[13] M. Arroyo, R. Zitzumbo, F. Avalos, Polymer **2000**, 41, 6351-6359.

[14] C.F. Antunes, A.V. Machado, M. van Duin, Eur. Polym. J. **2011**, 47, 1447-1459.

[15] V. Wal1, R. Nijhof, R.J. Gaymans, Polymer **1999**, 40, 6031-6044.

[16] X. Chen, J. Yu, Z. Luob, S. Guo, M. He, Z. Zhou, Polym. Adv. Technol. **2011**, 22, 657-663.

[17] W. Tang, J. Tang, H. Yuan, R. Jin, J. Appl. Polym. Sci. **2011**, 122, 461-468.

[18] P. Svoboda, R. Theravalappil, D. Svobodova, P. Mokrejs, K. Kolomaznik, K. Mori, T. Ougizawa, T. Inoue, Polym. Test. **2010**, 29, 742-748.

[19] C. Grein, M. Gahleitner, K. Bernreitner, eXPRESS Pol. Lett. **2012**, 6, 688-696.

[20] S. Chaput, C. Carrot, M. Castro, F. Prochazka, Rheol. Acta **2004**, 43, 417-426.

[21] R. Pucciariello, V. Villani, L. Guadagno, V. Vittoria, Polym. Eng. Sci. **2006**, 46, 1433-1442.

[22] D. Kaempfer, R. Thomann, R. Mulhaupt, Polymer **2002**, 43, 2909-2916.

[23] L.T. Truong, Å. Larsen, B. Holme, S. Diplas, F.K. Hansen, J. Roots, S. Jørgensen, Surf. Interface Anal. **2010**, 42, 1046-1049.

[24] J. Arranz-Andres, J. L. Guevara, T. Velilla, R. Quijada, R. Benavente, E. Perez , M. L. Cerrada, Polymer **2005**, 46, 12287-12297.

[25] Kimberly A. Chaffin, Frank S. Bates, Patrick Brant, Patent No: US006225412B1.

[26] http://rsbweb.nih.gov/ij/ (accessed 23.02.2012)

[27] H. Zhou, J. Ying, F. Liu, X. Xie, D. Li, Polym. Test. **2010**, 29, 640-647.

[28] Jun Li, Robert A. Shanks, Yu Long, J. Appl. Pol. Sci. **2003**, 87, 1179 –1189.

Captions

Figures

Figure 1. The complex viscosity and dynamic storage modulus vs. angular frequency for sPP and sPP blends with the blending ratio of 80/20 (A). Comparison of complex viscosity of various contents of elastomers at low angular frequency: sPP/EOC (B) and sPP/EPR (C). The storage modulus (G') at angular frequency 0.1 rad/s as a function of composition of sPP/EOC and sPP/EPR (D)

Figure 2. AFM micrographs of sPP/EOC blends at various compositions (wt/wt): 90/10 (A), 60/40 (B), 40/60 (C) and 20/80 (D)

Figure 3. AFM micrograph of sPP/EOC 80/20 blend.

Figure 4. AFM micrographs of sPP/EPR blends at various compositions (wt/wt): 90/10 (A), 80/20 (B), 60/40 (C) and 40/60 (D)

Figure 5. Image analysis for AFM micrographs of sPP/EOC (80/20) blend (A), sPP/EPR (80/20) blend (B) and sPP/EPR (60/40) (C).

Figure 6. Melting curves of sPP, EOC and EPR and blends

Figure 7. (A) Non-isothermal crystallization curves of sPP, EOC, EPR and blends. (B) Relative crystallinity as a function of temperature of sPP and blends.

Figure 8. Stress–strain curves of neat sPP and sPP blends at different testing temperatures.

Figure 9. Effect of EOC on tensile properties of sPP at different testing temperatures.

Figure 10. Effect of EPR on tensile properties of sPP at different testing temperatures.

Table

Table 1. Melt flow rate, density and flexural modulus of the polymers studied